Supporting Information

for

Achieving High Strength and High Ductility in Metal Matrix Composites Reinforced with Discontinuous Three-Dimensional Graphene-like Network

Xiang Zhang[a], Chunsheng Shi[a], Enzuo Liu[a,b], Fang He[a], Liying Ma[a], Qunying Li[a], Jiajun Li[a], Wolfgang Bacsa[d], Naiqin Zhao[*a,b,c] and Chunnian He[*a,b,c]

[a] *School of Materials Science and Engineering and Tianjin Key Laboratory of Composites and Functional Materials, Tianjin University, Tianjin, 300072, P. R. China*

[b] *Collaborative Innovation Center of Chemical Science and Engineering, Tianjin 300072, China*

[c] *Key Laboratory of Advanced Ceramics and Machining Technology, Ministry of Education, Tianjin University, Tianjin, 300072, China*

[d] *Université de Toulouse, UPS, CNRS, CEMES, 29 rue Jeanne Marvig, 31055 Toulouse, France*

* Address correspondence to

nqzhao@tju.edu.cn, cnhe08@tju.edu.cn

KEYWORDS: Metal matrix composites; graphene-like network; mechanical properties; strengthening; toughening

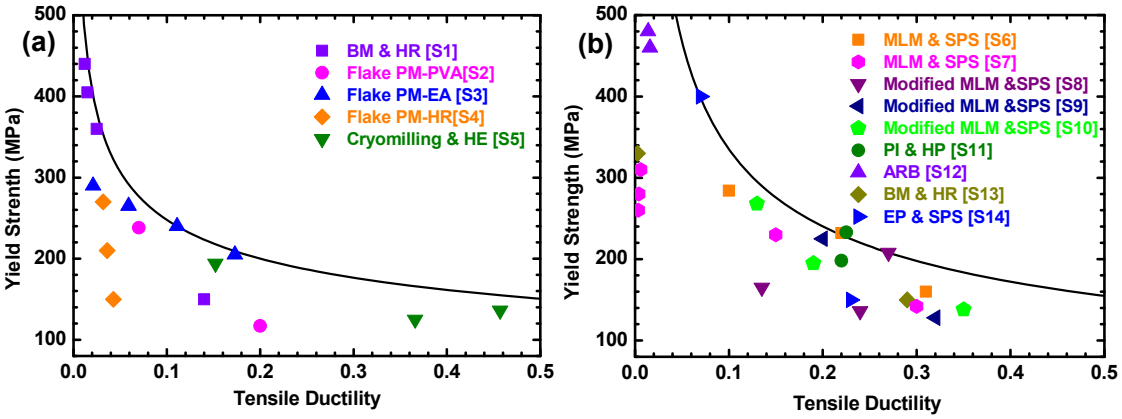

Figure S1. Yield strength versus total tensile elongation of the previously reported graphene (mainly rGO)-reinforced (a) Al and (b) Cu matrix composites.

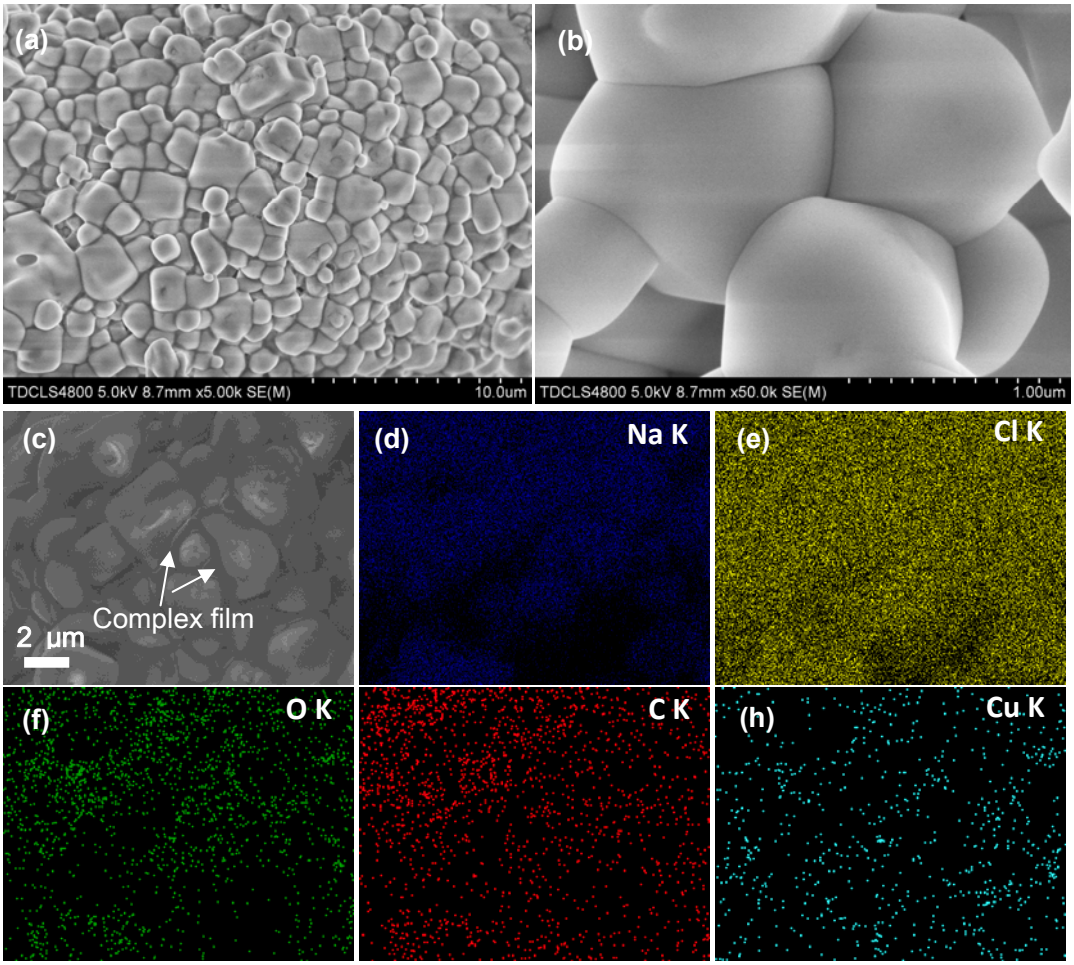

Figure S2. (a-c) SEM images of the assembled NaCl particles coated with ultrathin film of $Cu(NO_3)_2$-$C_6H_{12}O_6$ (NaCl@$Cu(NO_3)_2$-$C_6H_{12}O_6$) after freeze-drying process. (d-h) The corresponding EDX mappings of NaCl@$Cu(NO_3)_2$-$C_6H_{12}O_6$ shown in (c).

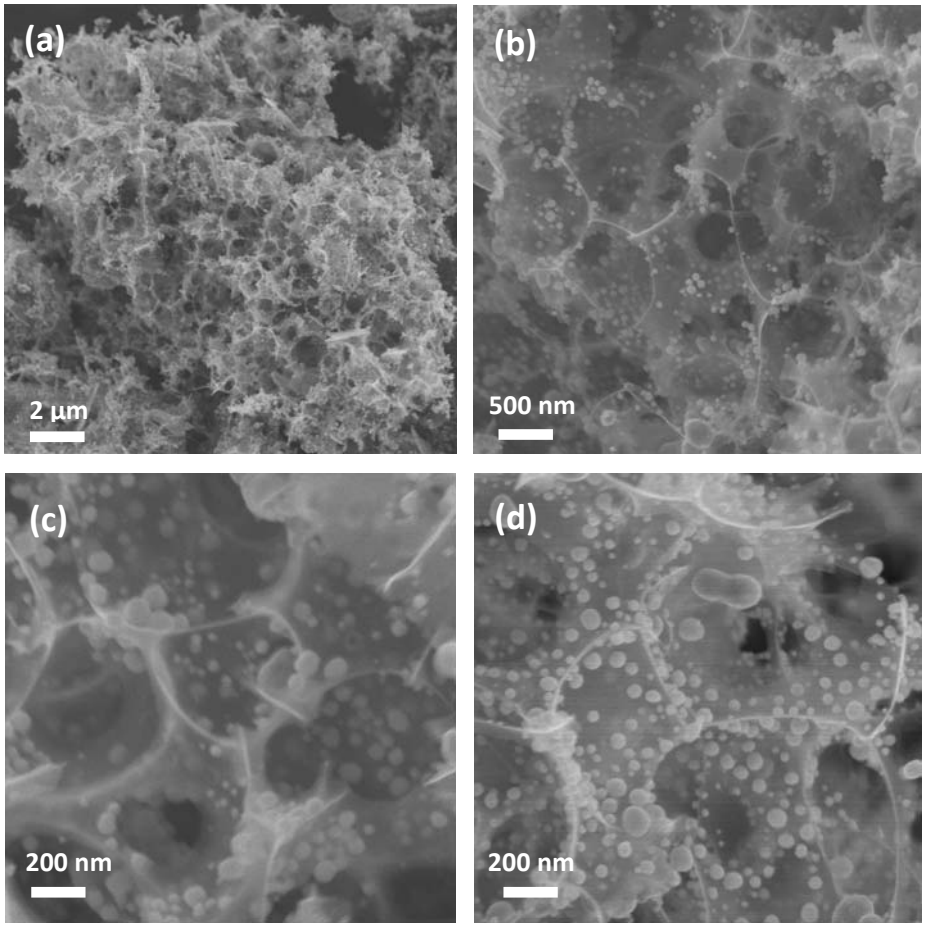

Figure S3. SEM images of 3D GN@Cu powders. The segregated network-like feature of 3D GN which replicates the surface of assembled NaCl particles could be observed clearly.

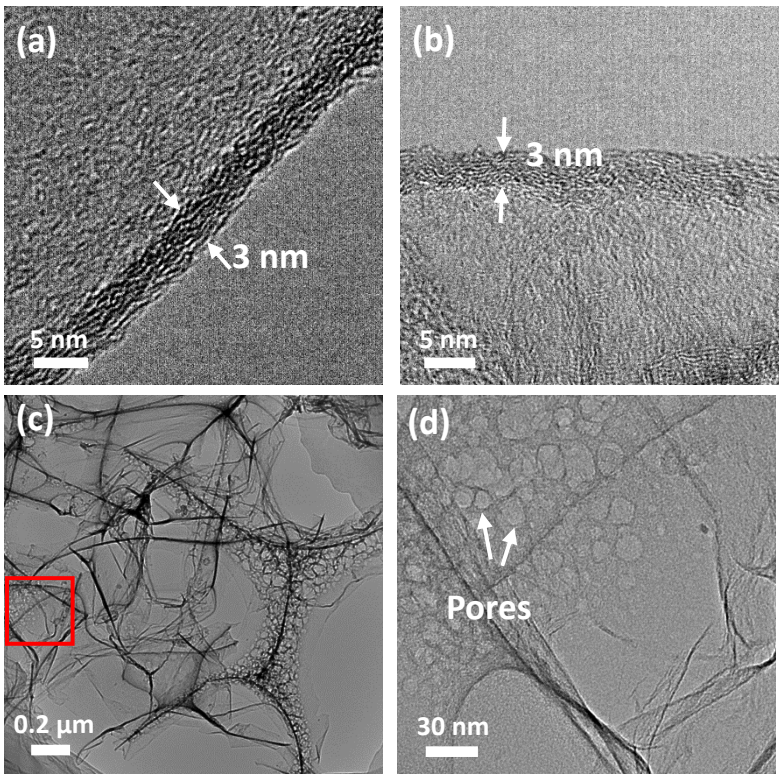

Figure S4. (a) and (b) HRTEM images of the edge of 3D GN, showing their uniform thickness of less than 3 nm. (c) and (d) TEM images of 3D graphene-like network after etching Cu NPs from the 3D GN@Cu powders. The pores in (d) suggesting a tight bonding between GN and Cu NPs formed during the heat-treatment process under H_2.

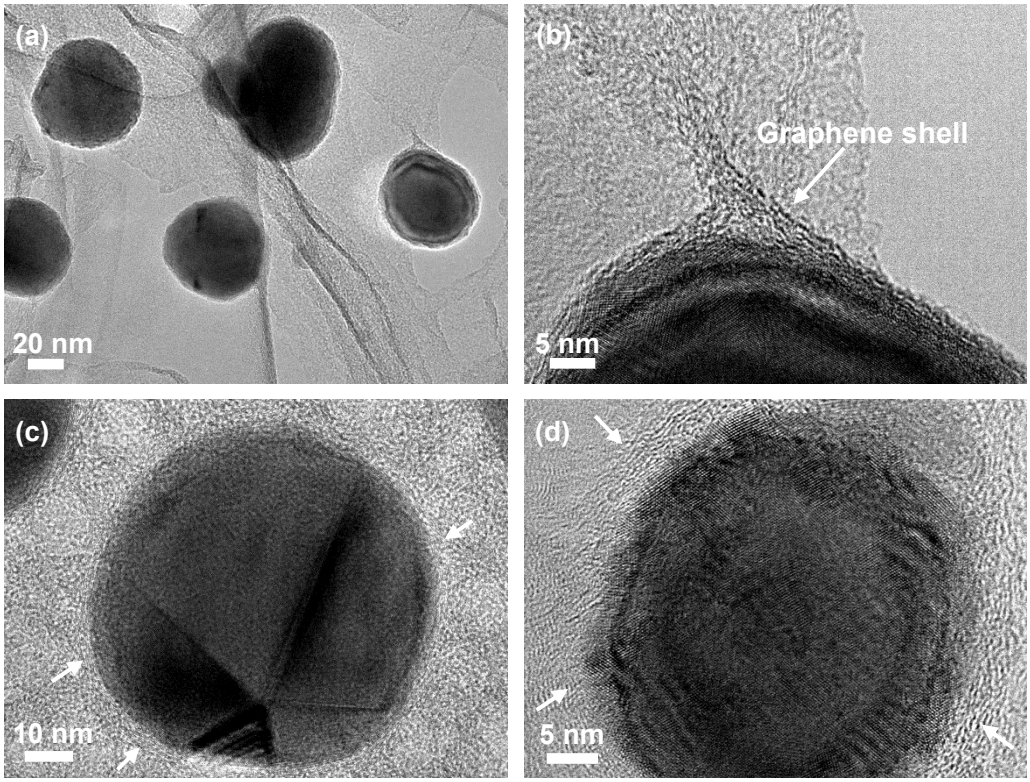

Figure S5. (a-d) HRTEM images of the 3D GN@Cu powders. Figure S4b shows a good evidence that Cu NP and GN have a reactive bonding on the interface. A thin layer of graphene-like shell around Cu NPs (indicated with arrows) could be observed in Figure S4c and d, indicating that the Cu NPs have good catalytic activity to transform carbon source nearby into graphene-like materials during the heat-treatment process under H_2, thus leading to a molecular level mixing between GN and Cu NPs.

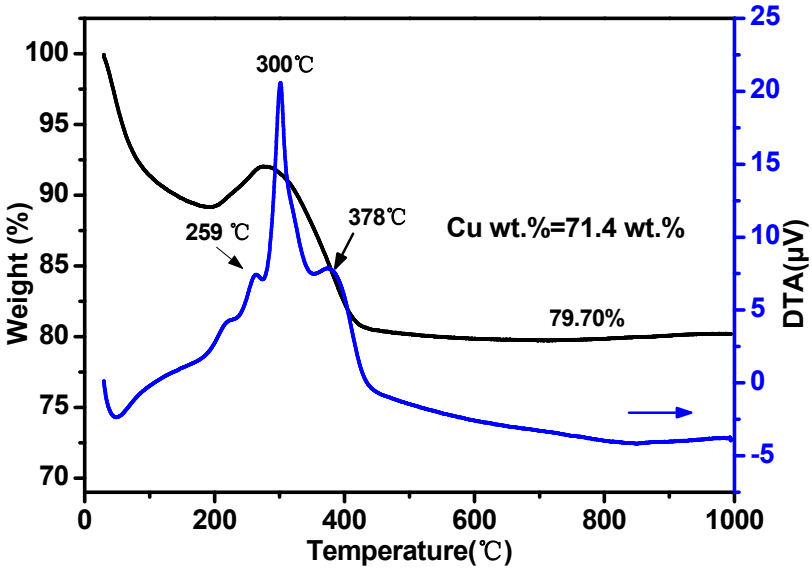

Figure S6. TGA and DTA thermal analyses for 3D GN@Cu powders. The original content of Cu was calculated to be 71.4 wt. % by calculating the final weight of CuO after heating the 3D GN@Cu powders in air atmosphere. The transition at 180 °C is due to the removal of water molecules and three exothermic peaks of the DTA curve at 259 °C，300 °C and 378 °C correspond to the following process Cu(s)→Cu_2O(s), C(s)→CO_2(g), and Cu_2O(s)→CuO(s), respectively. Compared with the reported thermal analysis about Cu NPs [S17, S18], an obvious shift to the higher temperature range of the two typical exothermic peaks could be observed in Figure S12, exhibiting good thermal stability for Cu NPs in the in-situ synthesised 3D GN@Cu. We speculated that it is because the rapid combustion of GN slowed down the oxidation rate of the tightly-bonded Cu NPs on its surface, in turn a decay in the appearance of the two exothermic peaks. The thermal analyses confirm the good stability of 3D GN@Cu in thermodynamics, which benefited by the close interfacial combination of unique in-situ synthesis process.

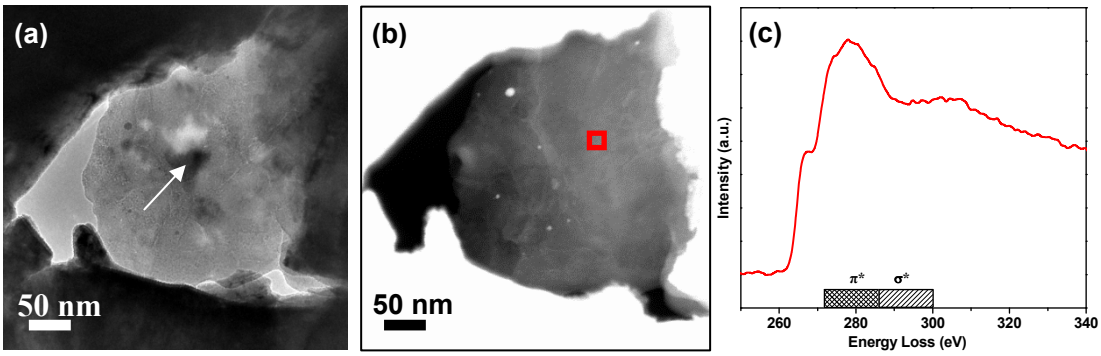

Figure S7. a) Bright field TEM image of 4.0 vol. % GN/Cu bulk composites and (b) High-angle annular dark field STEM image showing GN located in the center of the image that is in contact with the Cu region; (c) high-resolution electron energy loss spectroscopy (EELS) spectrum from carbon K-edge regions of the bright area in (b). Two peaks appearing at ~281 eV corresponding to transitions from 1s to the π* state and at ~291 eV related to transitions from 1s to σ* state. [S16]

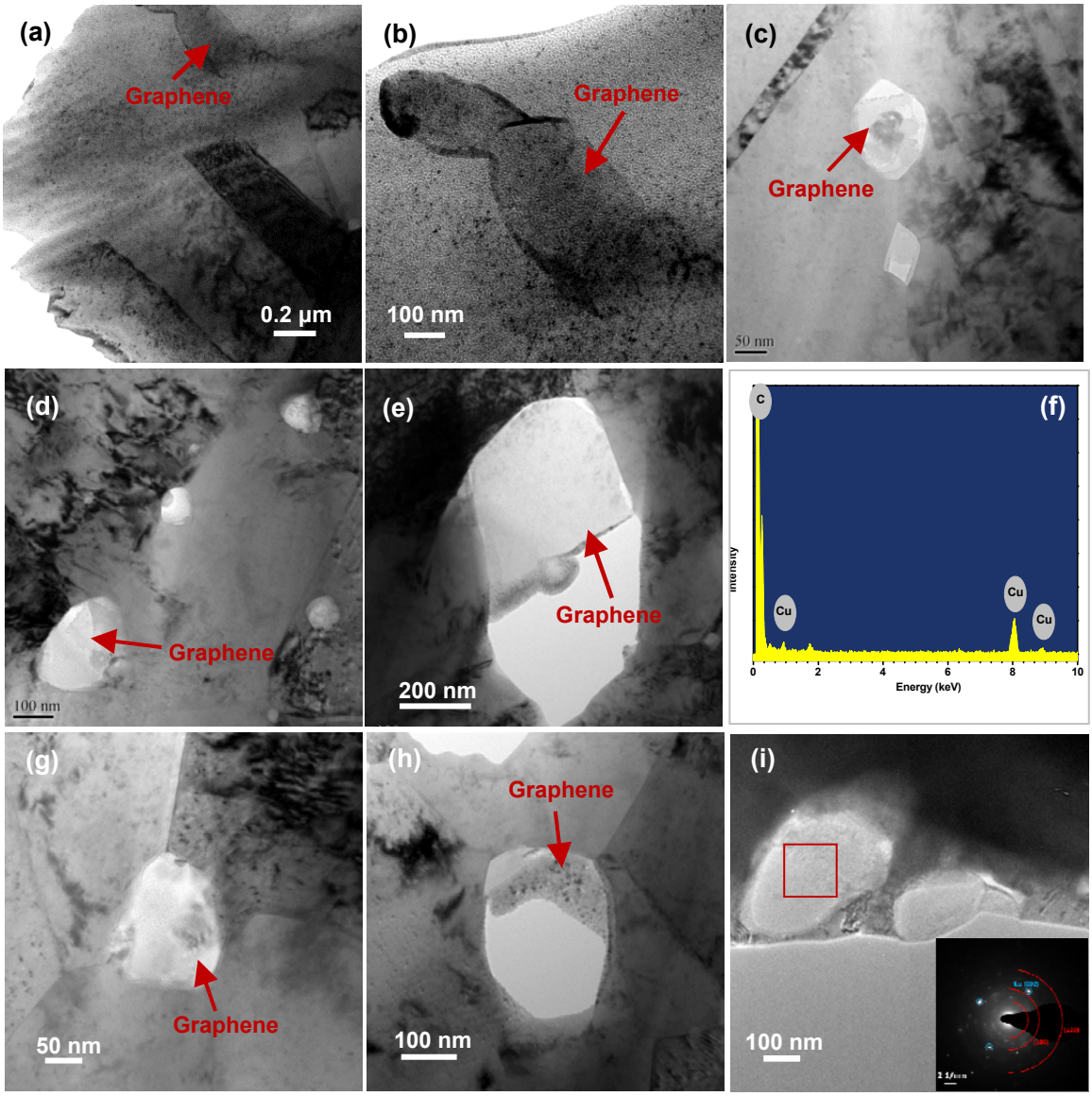

Figure S8. TEM images of 3D GN/Cu bulk composites, indicating that the graphene-like nanosheets are homogeneously dispersed in the grain interior (a, b, c, d) or crossing the grain boundary (e, g, h), as indicated by solid arrows in the images. (f) EDS spectrum of graphene-like nanosheets in image (e). (i) A typical image of the edge of the composites and the inset is the corresponding selected area electron diffraction (SAED) pattern, demonstrating the existence of Cu and graphene. As can be seen, the weak ring patterns were due to graphene, which confirmed (100) and (120) of graphene by calculating the interplanar spacing based on the radius (W.J.

Kim, et al. Carbon, 2016, 69, 55-65.; PDF#65-6212, graphite). The three bright spots were associated with Cu {002} (PDF #65-9026).

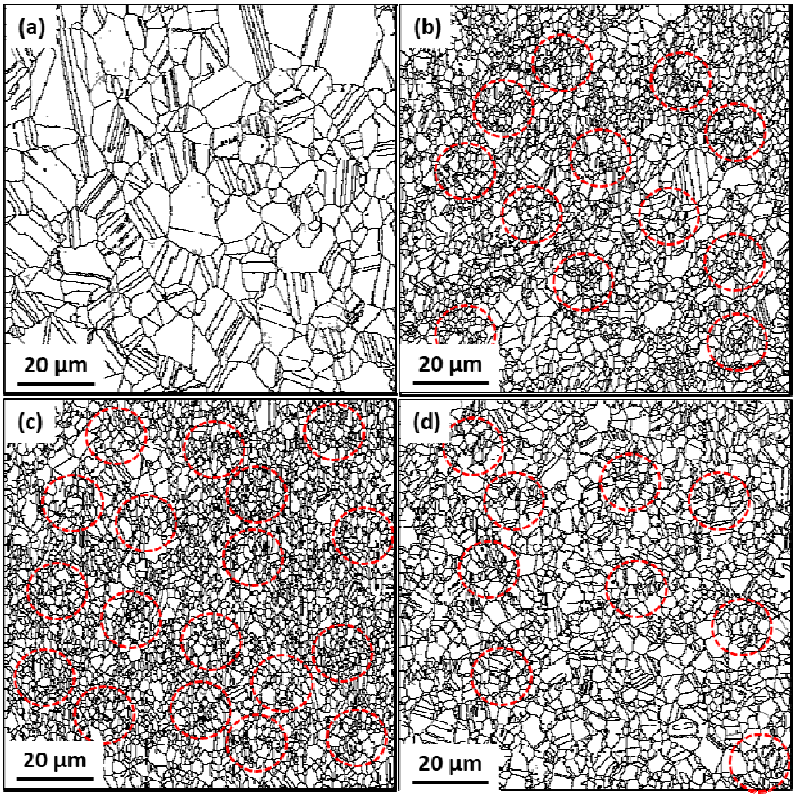

Figure S9. EBSD reconstruction map to show grain size. The interaction zones were highlighted by the red dotted box. In the interaction zone, the average grain size was apparently smaller than that of the outside grains.

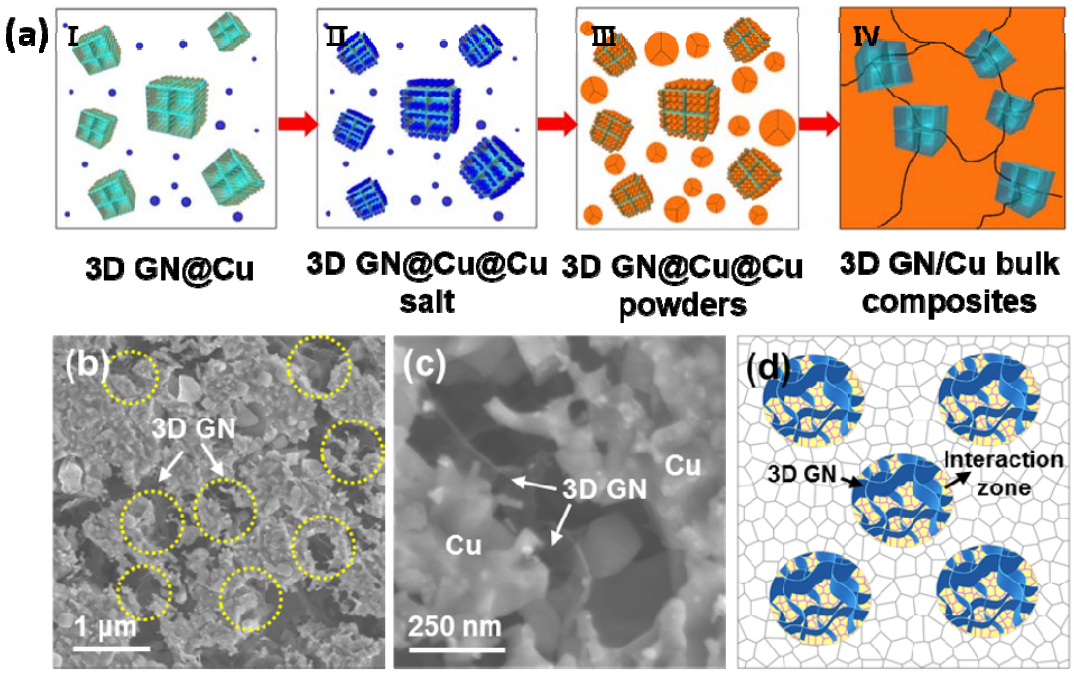

Figure S10. (a) The schematic illustration of the grain refinement mechanism in the 3D GN/Cu bulk composites. (Ⅰ) shows the initial stage of the impregnation process, demonstrating that the Cu NPs *in-situ* produced on the surface of 3D GN act as the adsorption sites for copper salt; (Ⅱ) exhibits the ending stage of the impregnation process, indicating the 3D GN@Cu fully encapsulated by the adsorbed copper salt; (Ⅲ) displays during the reduction process, 3D GN@Cu is wrapped by the Cu NPs reduced from the impregnated copper salt, leading to the formation of 3D GN@Cu@Cu powders; (Ⅳ) shows during the consolidation process, 3D GN dispersed near the Cu particle boundary and restrict the Cu grain growth. (b,c) SEM images of 4.0 vol. % bulk surface treated by etching agent, showing the distribution of 3D GN in the Cu matrix. d) Schematic of the distributions of 3D GN reinforcement and interaction zones.

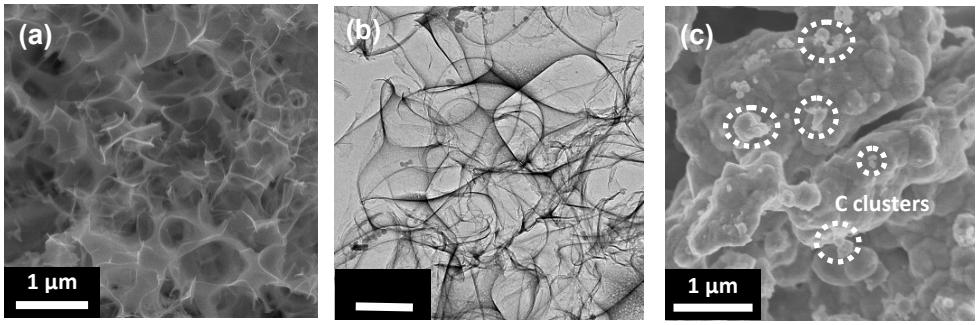

Figure S11. (a) SEM and (b) TEM images of 3D network-like carbon sheets (3D-CNS) synthesized by the same process without copper; (c) SEM image of the 3D-CNS after impregnation with copper nitrate methanol solution, carbon clusters could be observed.

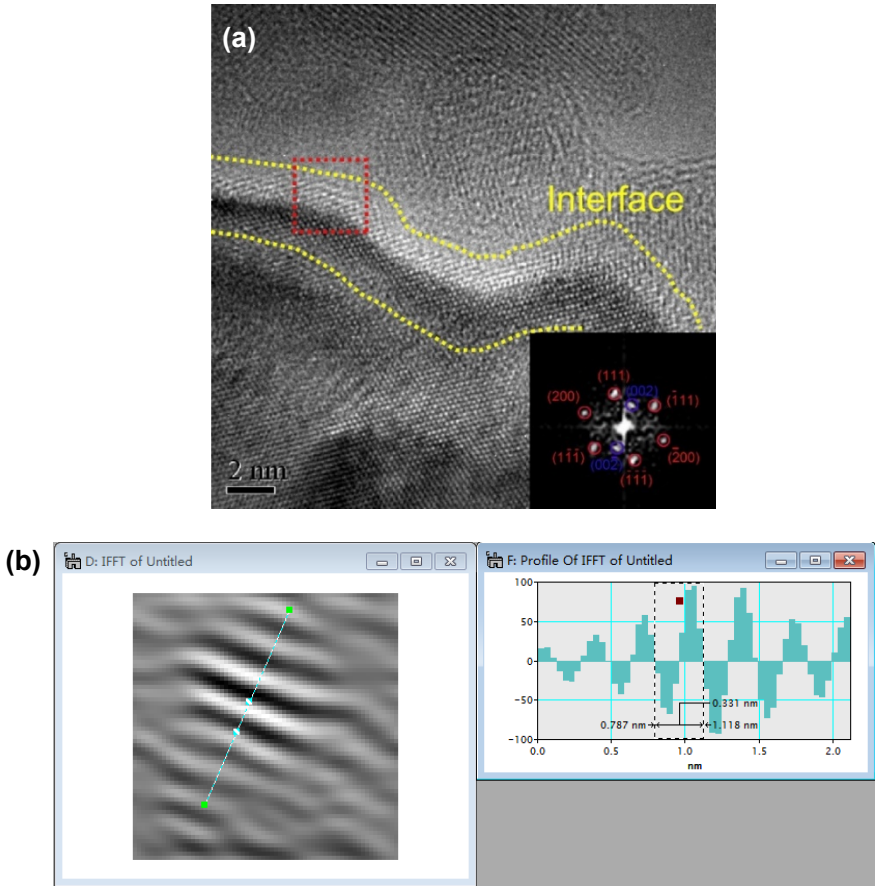

Figure S12. (a) An HRTEM image of the interface of GN and Cu matrix, inset is the FFT pattern of the corresponding selected area; (b) is the inverse FFT image (left) and

the corresponding lattice distance measurement data (right). The inverse FFT image indicates that there is a special crystallographic orientation relation between the graphene particles and Cu matrix: $\{110\}_{Cu} // \{002\}_{GN}$, the same crystallographic orientation was confirmed in a previous report [S11].

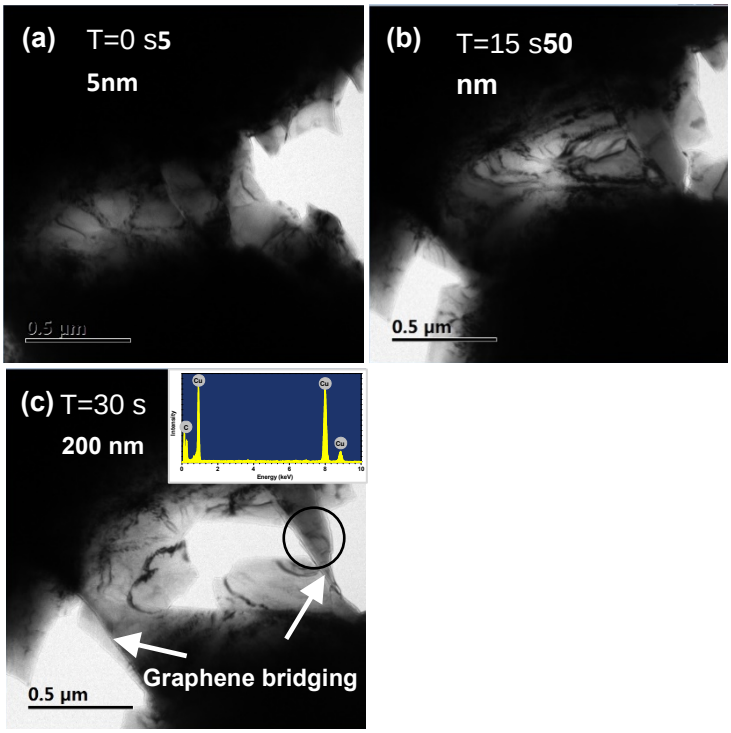

Figure S13. Screenshots of *in-situ* TEM tensile test of 3D GN/Cu bulk composites with 4.0 vol% graphene-like materials (Video S2), showing the hindrance on crack propagation and final fracture of the Cu matrix by the graphene-like nanosheets (marked with white arrows). Inset of (c) EDS spectrum of the area indicated with black circle.

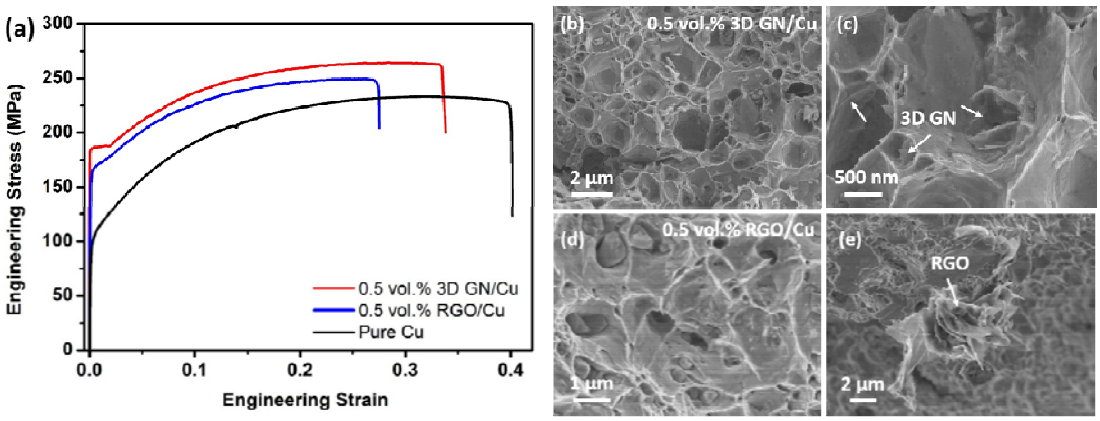

Figure S14. (a) Engineering stress-strain curves for 0.5 vol. % 3D GN/Cu composite, 0.5 vol.% rGO/Cu composite and pure Cu; SEM images of the fracture surface of (b,c) 0.5 vol. % 3D GN/Cu composites and (d, e) 0.5 vol.% rGO/Cu. The 0.5 vol.% rGO/Cu composite was fabricated with the same process with the 3D GN/Cu composite. The commercial GO used in this work was purchased from Nanjing XFNano Material Tech Co. Ltd., China.

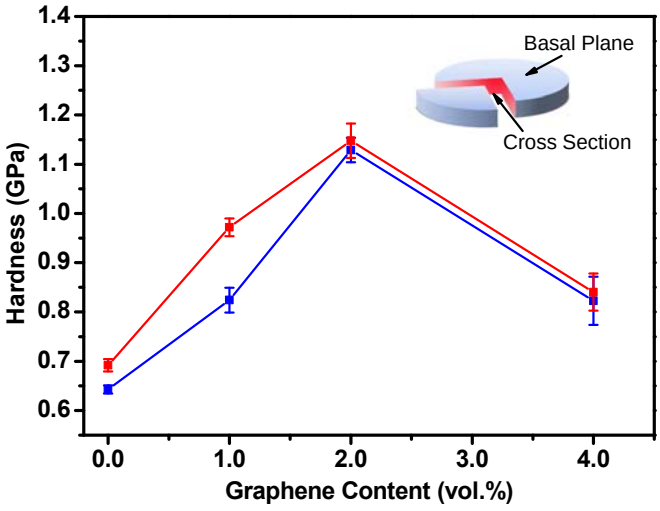

Figure S15. Vickers Hardness data of the basal plane (red curve) and cross section

(blue curve) of 3D GN/Cu bulk with different GN content.

Table S1. Yield strength and total tensile elongation data of Cu matrix composites in comparison with available literature.

Ref.	Reinfor-cement	Method	Graphene Content (vol. %)	Yield Strenth (MPa)	Tensile Ductility
14	**rGO**	Molecular Level Mixing (MLM) &SPS	0	160	0.310
			1.0	232	0.220
			2.5	284	0.100
15	**rGO**	Molecular Level Mixing & SPS	0	142	0.300
			0.2	230	0.150
			0.4	280	0.004
			0.6	310	0.006
			0.8	260	0.0035
18	**rGO**	modified molecular-level mixing	0	136	0.240
			0.1	208	0.270
20	**rGO**	Modified Molecular Level Mixing (one step reduction)& SPS	0	128	0. 320
			2.4	225	0.200
16	**rGO**	Modified Molecular Level Mixing(Ni NPs decorated)	0	138	0.350
			0.5	195	0.190
			1.0	268	0.130
17	**rGO**	preform impregnation & hot pressing (PI & HP)	0	106	0.180
			0.3	198	0.220
			1.2	233	0.225
19	**GN**	Accumulative Roll Bonding (ARB)	--	460	0.016
			--	480	0.014
29	**GN**	ball-milling & hot-rolling (BM-HR)	0	150	0.290
			11.1	330	0.0025
28	**rGO**	Electroless plating (EP) &SPS	0	150	0.230
			4.7	400	0.085
30	**CNTs**	Ball Milling & SPS & Cold rolling	0	135	0.140
			5.0	149	0.079
			10.0	197	0.065
31	**CNTs**	Ball milling & High-ratio differential speed rolling	0	358	0.207
			1.0	376	0.123
			3.0	417	0.122
32	**TiB_2**	Melt reaction &hot drawing	0	298.7	0.263
			6.67	509.6	0.074
33	**Y_2O_3**	Melt reaction	0	100	0.210
			0.9	490	0.050

34	Ti_3SiC_2	Electroless plating &Hot pressing	0	70	0.065
			5.0	182.7	0.022
			10.0	247.1	0.018

References

[S1] S. E. Shin, H. J. Choi, J. H. Shin, *Carbon* 2015, **82**, 143.

[S2] J. Wang; Z. Li, D. Fan, H. Pan, Z. Chen, D. Zhang, *Scr. Mater.* 2012, **66**, 594.

[S3] Z. Li, G. Fan, Q. Guo, Z. Li, Y. Su, D. Zhang, Carbon 2015, **95**, 419.

[S4] Z. Li, Q. Guo, Z. Q. Li, G. Fan, D. B. Xiong, Y. Su, J. Zhang, D. Zhang, *Nano Lett.* 2015, **15,** 8077.

[S5] J. L. Li, Y. C. Xiong, X. D. Wang, *Mater. Sci. Eng. A* 2015, **626**, 400.

[S6] J. Hwang, T. Yoon, S. H. Jin, J. Lee, T. S. Kim, S. H. Hong, S. Jeon, *Adv. Mater.* 2013, **25**, 6724.

[S7] F. Y. Chen, J. M. Ying, Y. F. Wang, S. Du, Z. Liu, Q. Huang, *Carbon*, 2016, **96**, 836.

[S8] D. D. Zhang; Z.J. Zhan, *J. Alloys Compd.* 2016, **654**, 226.

[S9] M. X. Li, J. Xie, Y. D. Li, H. H. Xu, *Physica Status Solidi (A)*, 2015, **212**, 2154.

[S10] Y. X. Tang, X. M. Yang, R. R. Wang, *Mater. Sci. Eng. A* 2014, **599**, 247.

[S11] D. B. Xiong, M. Cao, Q. Guo, Z. Tan, G. Fan, Z. Li, D. Zhang, *ACS Nano* 2015, **9**, 6934.

[S12] X. Liu, D. Wei, L. Zhuang, C. Cai, Y. Zhao, *Mater. Sci. Eng. A* 2015, **642**, 1.

[S13] P. Wang, W. Liu, L. Chen, *RSC Adv.* 2015, **5**, 51342.

[S14] C. Zhao, J. Wang, *Phys. Status Solidi A* 2014, **211**, 2878.

[S15] I. Shown, H. C. Hsu, Y. C. Chang, C. H. Lin, P. K. Roy, A. Ganguly, C. H. Wang, J. K. Chang, C. I. Wu, L. C. Chen, K. H. Chen, *Nano letters*, 2014, **14**, 6097.

[S16] L. Jiang, T. Z. Yang, F. Liu, J. Dong, Z. H. Yao, C. M. Shen, S. Z. Deng, N. S. Xu, Y. Q. Liu, H. J. Gao, *Adv. Mater.* 2013, **25**, 250.

[S17] I. Kim, Y. Kim, K. Woo, E. H. Ryu, K. Y. Yon, G. Z. Cao, J. Moon, *RSC Advances*, 2013, **3**, 15169.

[S18] M. I. Dar, S. Sampath, S. A. Shivashankar, *J. Mater. Chem.* 2012, **22**, 22418.